ROUGH CONOIDAL CRACK UNDER GENERAL LOADING : DISLOCATION, CRACK-TIP STRESS AND CRACK EXTENSION FORCE

P. N. B. ANONGBA

Université F. H. B. de Cocody, U. F. R. Sciences des Structures de la Matière et de Technologie, LASMES, 22 BP 582 Abidjan 22, Côte d'Ivoire

(reçu le 16 Novembre 2022; accepté le 26 Décembre 2022)

* Correspondance, e-mail : *anongba@gmail.com*

ABSTRACT

The rough conoidal crack is represented by a continuous distribution of dislocations with infinitesimal Burgers vectors. This is a smooth cone on average, and for definiteness, with a vertex O at the origin, vertical symmetrical axis, horizontal circular basis with radius $R = a$ at a height $x_2 = h(a)$. Its surface consists of profound striations running radially to the vertex. The rough conoidal crack dislocation at the elevation $x_2 = h(R)$ ($R \leq a$) is obtained as the intersection of a vertical cylinder of radius R (axis x_2) and the rough crack. The dislocation distribution consists of three families (m) (distribution function D_m; m= 1, 2 and 3) with burgers vectors b_m directed along the positive x_m-directions. The stresses are applied uniformly at infinity with tension σ_{22}^a along x_2 and shears σ_{21}^a and σ_{23}^a along x_1 and x_3. Poisson's normal stresses $-\nu\sigma_{22}^a$ (ν is Poisson's ratio) acting in the x_1 and x_3 directions are incorporated into the analysis. Plastic distortions associated with these dislocations are first given. Expressions of the elastic fields (displacement and stress) are also provided. Then distribution function $D_m^{(0)}$ of circular horizontal dislocations (with the identical Burgers vectors b_m) covering the smooth conoidal crack are considered and three singular integral equations that determine $D_m^{(0)}$ are written down. $D_m^{(0)} = D_m^{(0)}(\theta)$ depends on angle θ, complementary to the half angle at the vertex of the cone. $D_m^{(0)}$ may be used to approximate D_m. The crack-tip stresses have been given as functions of $D_m^{(0)}$. Explicit expressions of the rough circular crack extension force G_{RC} per unit length of the crack front are given that are associated with $D_m^{(0)}$ (θ = 0). Expressions $< G_{RC}^{(S)} >$ of $G_{RC}^{(S)}$ (crack extension force) averaged over the length of the oscillatory crack-front are

plotted for the special case of sinusoidal fronts. These plots reveal that the rough circular cracks can expand under small shearing stresses. Agreements are found with high cycle fatigue experiments.

Keywords : *fracture mechanics, linear elasticity, crack propagation and arrest, dislocations, crack extension force.*

RÉSUMÉ

Fissure conique rugueuse sous sollicitations extérieures arbitraires : dislocation, contrainte en tête de fissure et force d'extension de fissure

La fissure conoïdale rugueuse est représentée par une distribution continue de dislocations avec des vecteurs de Burgers infinitésimaux. C'est un cône lisse en moyenne, et pour la précision, de sommet *O* à l'origine, d'axe de symétrie vertical, de base circulaire horizontale de rayon $R = a$, à une hauteur $x_2 = h(a)$. Sa surface est constituée de stries profondes s'étendant radialement au vertex. La dislocation de fissure conoïdale rugueuse à l'élévation $x_2 = h(R)$ ($R \leq a$) est obtenue comme l'intersection d'un cylindre vertical de rayon R (axe x_2) et de la fissure rugueuse. La distribution des dislocations est composée de trois familles (m) (fonction de distribution Dm ; m = 1, 2 et 3) avec des vecteurs burgers b_m dirigés dans le sens positif des directions x_m. Les contraintes sont appliquées uniformément à l'infini avec une traction σ_{22}^a suivant x_2 et des cisaillements σ_{21}^a et σ_{23}^a selon x_1 et x_3. Les contraintes normales de Poisson $-\nu\sigma_{22}^a$ (ν est le rapport de Poisson) agissant dans les directions x_1 et x_3 sont intégrées à l'analyse. Les distorsions plastiques associées à ces dislocations sont d'abord données. Des expressions des champs élastiques (déplacement et contrainte) sont également fournies. Ensuite, les fonctions de distribution $D_m^{(0)}$ de dislocations horizontales circulaires (avec les mêmes vecteurs de Burgers b_m) couvrant la fissure conoïdale lisse sont considérées et trois équations intégrales singulières qui les déterminent sont écrites. $D_m^{(0)} = D_m^{(0)}(\theta)$ dépend de l'angle θ, complémentaire du demi-angle au sommet du cône. $D_m^{(0)}$ peut être utilisé pour approximer D_m. Les contraintes en tête de fissure ont été données en fonction de $D_m^{(0)}$. Des expressions explicites de la force d'extension de fissure circulaire rugueuse G_{RC}, par unité de longueur du front de fissure, sont données lesquelles sont associées à $D_m^{(0)}$ (θ = 0). Les expressions $< G_{RC}^{(S)} >$ de $G_{RC}^{(S)}$ (force d'extension de fissure) moyennées sur la longueur du front de fissure oscillatoire sont tracées pour le cas particulier des fronts sinusoïdaux. Ces tracés révèlent que les fissures circulaires rugueuses peuvent se dilater sous des contraintes de cisaillement faibles. Des accords sont trouvés avec des observations expérimentales en fatigue.

Mots-clés : *mécanique de la rupture, élasticité linéaire, propagation et arrêt de fissure, dislocation, force d'extension de fissure.*

I - INTRODUCTION

A recent work [1] has shown what follows: assume an elliptical crack of centre *O*, inside an infinitely extended isotropic elastic medium. The stresses are applied uniformly at infinity with tension σ_{22}^{a} along x_2 and shears σ_{21}^{a} and σ_{23}^{a} along x_1 and x_3. The plane of the crack is tilted around Ox_3 by an angle θ. The tension σ_{22}^{a} is in general out of the loop plane and provides positive values to $<G>$ the average crack extension force G per unit length of the crack front (averaged over all the positions on the crack front). The shears when parallel to the plane of the loop provide negative contributions. These suggest that an elliptical crack is unable to expand in its own plane under a shearing stress that lies in its plane. Shearing stresses provide positive values to $<G>$ only when they are inclined with respect to the plane of the crack loop. Under such conditions, the planar elliptic crack is not the right configuration to dealt with crack nucleation in brittle solids under applied mixed mode *I+II+III* loading (shearing stresses in the plane of the crack). We would have to start, from the beginning of crack expansion analysis, with a non-planar crack loop whose front should be locally of arbitrary shape. Consequently, it is more appropriate to investigate the expansion of the rough circular crack of mean radius *R* whose front lies on an edge-on cylinder (radius *R* and vertical axis). In other word, the front $\xi(P)$ (*i. e.* the vertical position of *P* with respect to the average crack front plane) of the rough crack at an arbitrary position *P*, lies on a vertical cylinder, and is expanded in the form of a Fourier series. By doing so the following crack problem that we call "the rough conoidal crack under general loading" is the subject of the present study. The rough conoidal crack is represented by a continuous distribution of rough circular crack dislocations. The elastic fields in the fractured medium read as a superposition of the elastic fields of the crack dislocations. ***Figure 1*** serves to illustrate the modelling. We consider an infinitely extended isotropic elastic medium containing in its interior a rough conoidal crack (vertex *O*, axis Ox_2 and height $h(a)= a\tan\theta$) whose basis is in the form of a rough circular line (centre *O'*, average radius $R = a$) displaced vertically from the origin *O* by $x_2= h(a)$. This rough crack is made of three families *j* (*j*= 1, 2 and 3) of rough circular crack dislocations with Burgers vectors b_j along x_j. ***Figure 1*** gives an illustration of a crack dislocation of arbitrary shape ξ located at the elevation $h= h(R)$ in the crack dislocation distribution.

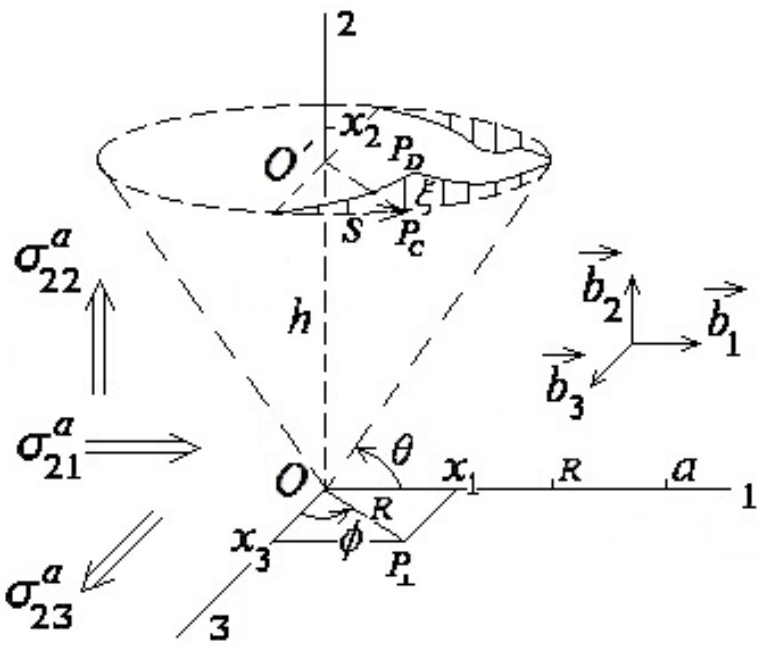

Figure 1 : *Schematic illustration of a rough conoidal crack dislocation (Burgers vectors b_j along x_j, j= 1, 2 and 3) at the elevation h= $h(R)$ in the dislocation distribution of a rough conoidal crack with vertex O, axis Ox_2, average radius and height $R = a$ and $h(a) = a\tan\theta$. In this geometry, applied loadings correspond to tension σ_{22}^a along x_2 and shears σ_{21}^a and σ_{23}^a along x_1 and x_3; see text for details*

The running point P_D along the dislocation is given with respect to (O, x_j) by

$$\overrightarrow{OP}_D = \begin{pmatrix} x_1 = R\sin\phi \\ x_2 = f = \sum_n A_n(R,\phi) + h(R) \equiv \xi + h \\ x_3 = R\cos\phi \end{pmatrix} \qquad (1a)$$

assuming that $A_n(R,\phi) = \xi_n(R)\sin\kappa_n|S|$; here n is a positive integer, κ_n and ξ_n (small in magnitude) are wave number and amplitude depending on R. S= $R\phi$ is the curvilinear abscissa of P_C (vertical projection of P_D on x_1x_3); $S \geq 0$ for $0 \leq \phi \leq \pi$ and $S \leq 0$ for $-\pi \leq \phi \leq 0$. We shall impose the condition $\sin\kappa_n|S| = 0$ for ϕ = 0 and $\pm\pi$ that gives $\kappa_n R \equiv n$ positive integer. In this way, the series form of ξ in $\overrightarrow{OP}_D$ (1*a*) reads

$$\xi = \sum_n \xi_n(R)\sin n|\phi|. \qquad (1b)$$

$h(R) = R\tan\theta$ and $0 < R \le a$. Only positions P_D with positive ϕ values are illustrated ***(Figure 1)***. We have $OO' = h(R)$; P_C and $P_\perp$ are the projections along x_2 of P_D on horizontal planes $x_2 = h(R)$ and $x_2 = 0$; θ is the angle complementary to the half angle at the vertex of average conoidal crack surface ($0 \le \theta \le \pi/2$). The medium is stressed uniformly at infinity with a tension σ_{22}^a in the vertical x_2- direction and shears σ_{21}^a and σ_{23}^a (parallel to the horizontal x_1x_3- plane) in the x_1 and x_3 directions. Distribution functions D_j of the crack dislocation j are defined such that $D_j(R)dR$ represents the number of dislocations j, in a small interval dR location at the position $x_1 = R$ on the Ox_1- axis ($-a < R < a$); $D_j(R) = D_j(-R)$, by symmetry, this restricts ourselves to positive x_1 values. The elastic fields (displacement $\vec{u}^{(j)}$ and stress $(\sigma)^{(j)}$) of the dislocation j located at $x_1 = R$ and average elevation $x_2 = h(R)$, in the rough conoidal crack dislocation distribution, may be deduced from those due to a rough circular sinusoidal dislocation located on average on Ox_1x_3 ($h = 0$) and defined by $x_2 = A_n(R, \phi) = \xi_n(R)\sin n|\phi|$ (identical Burgers vector $\vec{b}_j$). For the later, the elastic fields at $\vec{x} = (x_1, x_2, x_3)$ are (to linear term in ξ_n)

$$\vec{u}^{(j)(n)}(\vec{x}) = \vec{u}^{(j)(0)} + \vec{u}^{(j)A_n}$$
$$(\sigma)^{(j)(n)}(\vec{x}) = (\sigma)^{(j)(0)} + (\sigma)^{(j)A_n} \qquad (2)$$

$\vec{u}^{(j)(0)}$ and $(\sigma)^{(j)(0)}$ are of zero order corresponding to the fields due to a circular dislocation with centre O at the origin, radius R in the horizontal Ox_1x_3 plane with Burgers vector $\vec{b}_j$; these are available in [1]; $\vec{u}^{(j)A_n}$ and $(\sigma)^{(j)A_n}$ are oscillating parts involving ξ_n. When the dislocation exhibits shape (1), the elastic fields take the forms

$$\vec{u}^{(j)}(\vec{x}) = \vec{u}^{(j)(0)}(x_1, y_2, x_3) + \sum_n \vec{u}^{(j)A_n}(x_1, y_2, x_3) \equiv \vec{u}^{(j)(0)} + \vec{u}^{(j)\xi}$$
$$(\sigma)^{(j)}(\vec{x}) = (\sigma)^{(j)(0)}(x_1, y_2, x_3) + \sum_n (\sigma)^{(j)A_n}(x_1, y_2, x_3) \equiv (\sigma)^{(j)(0)} + (\sigma)^{(j)\xi} \qquad (3)$$

$y_2 = x_2 - h$. Elastic fields of rough conoidal crack dislocations ***(Figure 1)*** have not been reported. We shall provide expressions for these using the method called "Method of Fourier series or integrals" in review works by Mura [2, 3]: the method consists in writing the plastic distortions associated with the

dislocation in Fourier integral series forms. The displacement associated with a single wave (*i.e.*, simple sinusoidal) plastic distortion is available from [2, 3]. Those of the crack dislocations are derived by superposition. In *Section* 2 (Methodology), the procedures for determining the elastic fields of the dislocations and crack analysis are explained. In *Section* 3, are listed the elastic fields (stress and displacement) of the dislocations *j*, distribution functions D_j of crack dislocations, crack-tip stress, and crack extension force *G* per unit length of the crack front. *Section* 4 and 5 are devoted to discussion of the results and conclusion, respectively.

II - METHODOLOGY

II-1. Plastic distortions and elastic fields of rough conoidal crack dislocations

The three types *j* (*j* = 1, 2 and 3) of crack dislocation considered have Burgers vectors $\vec{b}_1 = (b,0,0)$, $\vec{b}_2 = (0,b,0)$ and $\vec{b}_3 = (0,0,b)$ along x_j; they spread on vertical cylinders (axis Ox_2, radii *R* with $0 < R \leq a$) with running point P_D coordinates given by (1) ***(Figure 1)***. We shall make use of the displacement $\bar{u}_m(\vec{x})$, *m*=1, 2 and 3, (see (5) below) due to a plastic distortion $\beta^*_{ij}(\vec{x})$ given as a periodic function of coordinates $\vec{x} = (x_1, x_2, x_3)$

$$\beta^*_{ij} = \bar{\beta}^*_{ij}(\vec{k}) e^{i\vec{k}.\vec{x}} \tag{4}$$

where $\vec{k} = (k_1, k_2, k_3)$ with k_j arbitrary constants. Mura [2, 3] has shown the associated displacement component to be

$$\bar{u}_m(\vec{x}) = -ik_l C_{klji} L_{mk} \bar{\beta}^*_{ij} e^{i\vec{k}.\vec{x}}. \tag{5}$$

For isotropic material,

$$L_{mk} = \frac{\delta_{km}(\lambda + 2\mu)k^2 - k_k k_m(\lambda + \mu)}{\mu(\lambda + 2\mu)k^4} \tag{6}$$

where $k^2 = k_1^2 + k_2^2 + k_3^2$ and

$$C_{klji} = \lambda\delta_{kl}\delta_{ji} + \mu\delta_{kj}\delta_{li} + \mu\delta_{ki}\delta_{lj}, \tag{7}$$

δ_{ij} being the Kronecker delta and λ and μ are Lamé's constants. The non-zero plastic distortions $\beta_{rs}^{*(j)}$ associated with a rough circular dislocation j in Ox_1x_3 on average, centred at the origin with radius R and running point coordinates $x_2 = A_n \equiv \xi_n(R)\sin n\phi$ (see (1) for the others) take the forms (at arbitrary spatial position $\vec{x} = (x_1, x_2, x_3)$)

$$\begin{aligned}
\beta_{21}^{*(1)} &= \frac{bR^2\sin^2\phi}{R^2\sin^2\phi + (\partial A_n/\partial\phi)^2}\delta(x_2 - A_n)\left(H[\rho_1] - H[\rho_2]\right) = \beta_{23}^{*(3)} \\
\beta_{31}^{*(1)} &= \frac{bR\sin\phi\partial A_n/\partial\phi}{R^2\sin^2\phi + (\partial A_n/\partial\phi)^2}\delta(x_2 - A_n)\left(H[\rho_1] - H[\rho_2]\right) = \beta_{33}^{*(3)} \\
\beta_{12}^{*(2)} &= bH(x_2 - A_n)\left(\delta[\rho_1] - \delta[\rho_2]\right) \\
\beta_{32}^{*(2)} &= bH(x_2 - A_n)\left(\delta\left[x_3 + \sqrt{R^2 - x_1^2}\right] - \delta\left[x_3 - \sqrt{R^2 - x_1^2}\right]\right)
\end{aligned} \tag{8}$$

where $\rho_1 = x_1 + \sqrt{R^2 - x_3^2}$, $\rho_2 = x_1 - \sqrt{R^2 - x_3^2}$, $0 \le \phi \le \pi$ and $R > 0$. δ and H are the Dirac delta function and Heaviside step function, respectively. To linear terms with respect to A_n and $\partial A_n/\partial\phi$, the plastic distortions of these crack dislocations j read

$$\beta_{rs}^{*(j)} = \beta_{rs}^{*(j)(0)} + \beta_{rs}^{*(j)A_n}. \tag{9}$$

Here $\beta_{rs}^{*(j)(0)}$ corresponds to the circular dislocation j in Ox_1x_3 with centre O and radius R the elastic fields ($\vec{u}^{(j)(0)}$ and $(\sigma)^{(j)(0)}$) of which are available (see [1]) and used in (3) to provide the zero order terms with respect to ξ_n in the elastic fields of the rough conoidal crack dislocation j with shape (1). $\beta_{rs}^{*(j)A_n}$ is the complementary term with ξ_n that is used with the help of (5) to provide $\vec{u}^{(j)A_n}$ and $(\sigma)^{(j)A_n}$ in (2) and (3). Their used Fourier forms are

$$\begin{aligned}
\beta_{21}^{*(1)A_n} = \frac{bR\xi_n}{4(2\pi)^3}\sum_{m_1,m_3=-\infty}^{\infty}(-1)^{m_1+m_3}i^{m_3+1}b_{21}^{*(1)}(n;m_1,m_3) \\
\times\int_{-\infty}^{\infty}\int_{-\infty}^{\infty}\int_{-\infty}^{\infty}\frac{k_2}{k_1}J_{m_1}[k_1R]J_{m_3}[k_3R]e^{i\vec{k}.\vec{x}}d\vec{k} = \beta_{23}^{*(3)A_n}
\end{aligned} \tag{10}$$

$$b_{21}^{*(1)}(n;m_1,m_3)=-8n[(-1)^{m_1+m_3+n}+1]\left(\frac{m_1+m_3}{\left[(m_1+m_3-n)^2-1\right]\left[(m_1+m_3+n)^2-1\right]}\right.$$
$$\left.+\frac{m_1-m_3}{\left[(m_1-m_3-n)^2-1\right]\left[(m_1-m_3+n)^2-1\right]}\right)\equiv-16n\bar{b}_{21}^{*(1)}(n;m_1,m_3) \qquad (11)$$

m_1 and m_3 are natural numbers taking positive and negative values, $d\vec{k}=dk_1\,dk_2\,dk_3$, J_{m_1} and J_{m_3} are Bessel functions of the first kind with arguments k_1R and k_3R, respectively.

$$\beta_{31}^{*(1)A_n}=\frac{ibR\xi_n\kappa_n}{2(2\pi)^3}\sum_{m_1,m_3=-\infty}^{\infty}(-1)^{m_1+m_3}i^{m_3+1}b_{31}^{*(1)}(n;m_1,m_3)$$
$$\times\int_{-\infty}^{\infty}\int_{-\infty}^{\infty}\int_{-\infty}^{\infty}\frac{1}{k_1}J_{m_1}[k_1R]J_{m_3}[k_3R]e^{i\vec{k}.\vec{x}}d\vec{k}=\beta_{33}^{*(3)A_n} \qquad (12)$$

$$b_{31}^{*(1)}=2[(-1)^{m_1+m_3+n}-1]\left(\frac{m_1+m_3}{(m_1+m_3)^2-n^2}+\frac{m_1-m_3}{(m_1-m_3)^2-n^2}\right)\equiv-4\bar{b}_{31}^{*(1)} \qquad (13)$$

$$\beta_{12}^{*(2)A_n}=\frac{bR\xi_n}{4(2\pi)^3}\sum_{m_1,m_3=-\infty}^{\infty}(-1)^{m_1+m_3}i^{m_3+1}b_{21}^{*(1)}(n;m_1,m_3)$$
$$\times\int_{-\infty}^{\infty}\int_{-\infty}^{\infty}\int_{-\infty}^{\infty}J_{m_1}[k_1R]J_{m_3}[k_3R]e^{i\vec{k}.\vec{x}}d\vec{k}\ , \qquad (14)$$

$$\beta_{32}^{*(2)A_n}=\frac{bR\xi_n}{4(2\pi)^3}\sum_{m_1,m_3=-\infty}^{\infty}(-1)^{m_1}i^{m_3}b_{32}^{*(2)}(n;m_1,m_3)$$
$$\times\int_{-\infty}^{\infty}\int_{-\infty}^{\infty}\int_{-\infty}^{\infty}J_{m_1}[k_1R]J_{m_3}[k_3R]e^{i\vec{k}.\vec{x}}d\vec{k} \qquad (15)$$

$$b_{32}^{*(2)}=i\left(1+(-1)^{m_3}\right)[(-1)^{m_1+m_3+n}+1]i^{m_1+m_3+n}\left(\frac{(-1)^{m_3}}{(m_3-m_1-n-1)(m_3-m_1-n+1)}\right.$$
$$-\frac{(-1)^{m_1}}{(m_3-m_1+n-1)(m_3-m_1+n+1)}+\frac{(-1)^n}{(m_3+m_1-n-1)(m_3+m_1-n+1)}$$
$$\left.-\frac{1}{(m_3+m_1+n-1)(m_3+m_1+n+1)}\right) \qquad (16)$$

The associated elastic fields $\vec{u}^{(j)A_n}$ and $(\sigma)^{(j)A_n}$ have been obtained with the help of (5). It is then possible to write down the elastic fields from (3) for the rough conoidal crack dislocation at the elevation $x_2 = h(R)$ in the rough crack dislocation distribution as illustrated in ***Figure 1***. The results are displayed in *Section* 3.

II-2. Crack analysis

Our crack model ***(Figure 1)*** has been described earlier in *Section* 1. In addition to the externally applied tension σ_{22}^a along x_2 and shears σ_{21}^a and σ_{23}^a along x_1 and x_3, induced Poisson's normal stresses $-\nu_A\sigma_{22}^a$ (ν_A is Poisson's ratio ν so denoted to track the contributions of Poisson's stress) acting in the x_1 and x_3 directions are incorporated into the analysis. The traction-free boundary condition at any spatial position of the fracture surface is required:

$$\begin{cases} \bar{\sigma}_{12} - \partial f / \partial x_1 \bar{\sigma}_{11} - \partial f / \partial x_3 \bar{\sigma}_{13} = 0 \\ \bar{\sigma}_{22} - \partial f / \partial x_1 \bar{\sigma}_{12} - \partial f / \partial x_3 \bar{\sigma}_{23} = 0 \\ \bar{\sigma}_{23} - \partial f / \partial x_1 \bar{\sigma}_{13} - \partial f / \partial x_3 \bar{\sigma}_{33} = 0 \end{cases} \tag{17}$$

$\bar{\sigma}_{ij}$ stands for the total stress at any point $P(x_1, x_2, x_3)$ in the medium and is linked to the rough crack dislocation distribution D_j. (17) concerns the positions on the crack faces only. $\bar{\sigma}_{ij}$ is written as

$$\bar{\sigma}_{ij} = \sigma_{ij}^A + \sigma_{ij}^{(C)(1)} + \sigma_{ij}^{(C)(2)} + \sigma_{ij}^{(C)(3)} \tag{18}$$

$(\sigma)^A$ is the externally applied stress including normal induced stresses from Poisson effect,

$$(\sigma)^A = \begin{pmatrix} -\nu_A\sigma_{22}^a & \sigma_{12}^a & 0 \\ \sigma_{12}^a & \sigma_{22}^a & \sigma_{23}^a \\ 0 & \sigma_{23}^a & -\nu_A\sigma_{22}^a \end{pmatrix} \tag{19}$$

$$\sigma_{ij}^{(C)(m)}(\vec{x}) = \int_0^a \sigma_{ij}^{(m)}(\vec{x}; R) D_m(R) dR \qquad (m = 1, 2 \text{ and } 3) \tag{20}$$

$\sigma_{ij}^{(m)}$ is the stress field at $\vec{x}$ due to a conoidal rough crack dislocation m with position $x_1 = R$ along x_1 in the distribution. (17) give three integral equations

the resolution of which yields the D_m. The relative displacements ϕ_m of the faces of the crack in the x_m-direction at the position P_D (1a) in the distribution are obtained by integration from the relation $d\phi_m = -bD_m(R)dR$:

$$\phi_m = \int_R^a bD_m(R')dR', \qquad 0 \le R \le a \text{ and } 0 \le \phi \le \pi . \tag{21}$$

Special cracks captured by the modelling are the conoidal smooth crack (ξ = 0) and the rough conoidal crack with a sinusoidal front $\xi = \xi_n \sin n|\phi|$ (n= 1, 2 …). From (18) to (20), one can obtain the crack-tip stresses. The crack extension force G per unit length of the crack front is defined in previous works (see [1, 4 – 9], for example). The presentations in [1, 7] best correspond to the present case. The front of the rough crack ***(Figure 1)*** with shape (say P_D, (1)) at (R, ϕ) is assumed to advance quasi statically from (R= a, ϕ) (shorter crack) to (R= a+δa, ϕ) (lengthened crack). At an arbitrary position $P_D(x_1, x_2, x_3)$ (1) with $a \le R \le a+\delta a$, is attached a surface element $\overrightarrow{ds}$ that reads

$$\overrightarrow{ds} = \begin{pmatrix} ds_1 \\ ds_2 \\ ds_3 \end{pmatrix} = dRd\phi \begin{pmatrix} -x_1 \dfrac{\partial x_2}{\partial R} - \dfrac{x_3}{R}\dfrac{\partial x_2}{\partial \phi} \\ R \\ \dfrac{x_1}{R}\dfrac{\partial x_2}{\partial \phi} - x_3 \dfrac{\partial x_2}{\partial R} \end{pmatrix} \tag{22}$$

The component of the force acting on ds in the x_i – direction is $\bar{\sigma}_{ij} ds_j$ (the summation convention on repeated subscripts applies) where $\bar{\sigma}_{ij}$ are stresses ahead of the shorter or behind the lengthened crack; thus the energy change associated with ds is $\bar{\sigma}_{ij} ds_j \Delta u^{(i)}/2$ (here a summation is also considered over i = 1, 2 and 3) where $\Delta u^{(i)}$ is the difference in displacement across the lengthened crack, just behind its tip, in the x_i – direction. When the crack advances from $R = a$ to $a + \delta a$, the energy decrease associated with a surface element

$$\Delta s = \int_{R=a}^{a+\delta a} ds(P_D) \cong a\delta a d\phi \sqrt{1 + (\partial x_2(P_0)/\partial R)^2 + (\partial x_2(P_0)/\partial S)^2} \tag{23}$$

(δa being small and, when used below, will be let to go to zero) is given as

$$-\delta E = \frac{1}{2}\int_{a}^{a+\delta a}\sum_{i}\sum_{j}\bar{\sigma}_{ij}\,ds_j\,\Delta u^{(i)}\,, \tag{24}$$

the integration being performed with respect to R; we stress that Δs is the sum of the surface elements ds taken at the various points P_D (1) as R only changes from a to $a+\delta a$. The crack extension force per unit length of the crack front at $P_0 = P_D$ (with $R = a$, ϕ given) is defined as

$$G(P_0) = \lim_{\delta a \to 0} -\delta E / \Delta s\,. \tag{25}$$

III - RESULTS

III-1. Elastic fields of rough conoidal crack dislocations

Referring to (3), *Section* 2, we obtain

$$\frac{u_1^{(1)A_n}(\vec{x})}{u_0(R)} = \sum_{m_1=1}^{\infty}\left((-1)^{m_1}-1\right)\Bigg(\Bigg\|-b_{21}^{*(1)}(n;m_1,m_3=0)\Bigg[2(1-\nu)\frac{\partial^2}{\partial x_2^2}$$

$$-\frac{\partial^2}{\partial x_1^2}-y_2\frac{\partial^3}{\partial x_2\partial x_1^2}\Bigg]+4(1-\nu)\kappa_n b_{31}^{*(1)}(n;m_1,m_3=0)\frac{\partial}{\partial x_3}\Bigg\|B_2^{*(1)}(m_1,m_3=0)$$

$$+i2\kappa_n b_{31}^{*(1)}(n;m_1,m_3=0)\frac{\partial^2}{\partial x_3\partial x_1}\left[1-y_2\frac{\partial}{\partial x_2}\right]B_1^{*(1)}(m_1,m_3=0)$$

$$-\sum_{m_3=1}^{\infty}2i^{m_3}(-1)^{m_3}\Bigg\{\Bigg\|b_{21}^{*(1)}(n;m_1,m_3)\Bigg[2(1-\nu)\frac{\partial^2}{\partial x_2^2}-\frac{\partial^2}{\partial x_1^2}-y_2\frac{\partial^3}{\partial x_2\partial x_1^2}\Bigg]$$

$$-4(1-\nu)\kappa_n b_{31}^{*(1)}(n;m_1,m_3)\frac{\partial}{\partial x_3}\Bigg\|B_2^{*(1)}(m_1,m_3)-i2\kappa_n b_{31}^{*(1)}(n;m_1,m_3)$$

$$\times\frac{\partial^2}{\partial x_3\partial x_1}\left[1-y_2\frac{\partial}{\partial x_2}\right]B_1^{*(1)}(m_1,m_3)\Bigg\}\Bigg),$$

$$\frac{u_2^{(1)A_n}(\vec{x})}{u_0(R)} = \sum_{m_1=1}^{\infty}\left((-1)^{m_1}-1\right)\Bigg(i\Bigg\|b_{21}^{*(1)}(n;m_1,m_3=0)\Bigg[2\nu\frac{\partial}{\partial x_2}+y_2\frac{\partial^2}{\partial x_2^2}\Bigg]$$

$$-2\kappa_n b_{31}^{*(1)}(n;m_1,m_3=0)y_2\frac{\partial}{\partial x_3}\Bigg\|B^{*(2)}(m_1,m_3=0)$$

$$+\sum_{m_3=1}^{\infty}2i^{m_3+1}(-1)^{m_3}\Bigg\|b_{21}^{*(1)}(n;m_1,m_3)\Bigg[2\nu\frac{\partial}{\partial x_2}+y_2\frac{\partial^2}{\partial x_2^2}\Bigg]$$

$$-2\kappa_n b_{31}^{*(1)}(n;m_1,m_3)y_2\frac{\partial}{\partial x_3}\Big\|B^{*(2)}(m_1,m_3)\Big)\,,$$

$$\frac{u_3^{(1)A_n}(\vec{x})}{u_0(R)}=\sum_{m_1=1}^{\infty}\Big((-1)^{m_1}-1\Big)\Bigg(i\Bigg\{\Big\|b_{21}^{*(1)}(n;m_1,m_3=0)\frac{\partial}{\partial x_3}\Big[1+y_2\frac{\partial}{\partial x_2}\Big]$$

$$+4(1-\nu)\kappa_n b_{31}^{*(1)}(n;m_1,m_3=0)\Big\|B^{*(2)}(m_1,m_3=0)$$

$$+2\kappa_n b_{31}^{*(1)}(n;m_1,m_3=0)\frac{\partial^2}{\partial x_3^2}\Big[1-y_2\frac{\partial}{\partial x_2}\Big]B_1^{*(1)}(m_1,m_3=0)\Bigg\}$$

$$+\sum_{m_3=1}^{\infty}2i^{m_3+1}(-1)^{m_3}\Bigg\{\Big\|b_{21}^{*(1)}(n;m_1,m_3)\frac{\partial}{\partial x_3}\Big[1+y_2\frac{\partial}{\partial x_2}\Big]$$

$$+4(1-\nu)\kappa_n b_{31}^{*(1)}(n;m_1,m_3)\Big\|B^{*(2)}(m_1,m_3)+2\kappa_n b_{31}^{*(1)}(n;m_1,m_3)$$

$$\times\frac{\partial^2}{\partial x_3^2}\Big[1-y_2\frac{\partial}{\partial x_2}\Big]B_1^{*(1)}(m_1,m_3)\Bigg\}\Bigg)\,; \qquad (26)$$

$$B_2^{*(1)}(m_1,m_3)=\int_{-\infty}^{\infty}\int_{-\infty}^{\infty}\frac{e^{-|y_2|\eta_1}}{\eta_1}\frac{J_{m_1}[k_1R]}{k_1}J_{m_3}[k_3R]e^{i(k_1x_1+k_3x_3)}dk_1dk_3\,,$$

$$B_1^{*(1)}(m_1,m_3)=\int_{-\infty}^{\infty}\int_{-\infty}^{\infty}\frac{e^{-|y_2|\eta_1}}{\eta_1^3}J_{m_1}[k_1R]J_{m_3}[k_3R]e^{i(k_1x_1+k_3x_3)}dk_1dk_3\,,$$

$B^{*(2)}=-i\frac{\partial B_2^{*(1)}}{\partial x_1}$, $\eta_1^2=k_1^2+k_3^2$, $B_1^{*(1)}=-i\frac{\partial B_3^{*(1)}}{\partial x_1}$ (used below) and

$$u_0(R)=\frac{bR\xi_n}{16(2\pi)^2(1-\nu)}\ . \qquad (27)$$

$$\frac{u_1^{(3)A_n}(\vec{x})}{u_0(R)}=\sum_{m_1=1}^{\infty}\Big((-1)^{m_1}-1\Big)\Bigg(i\Bigg\{\Big\|b_{21}^{*(1)}(n;m_1,m_3=0)\frac{\partial}{\partial x_3}\Big[1+y_2\frac{\partial}{\partial x_2}\Big]$$

$$+4\nu\kappa_n b_{31}^{*(1)}(n;m_1,m_3=0)\Big\|B^{*(2)}(m_1,m_3=0)+2\kappa_n b_{31}^{*(1)}(n;m_1,m_3=0)$$

$$\times\frac{\partial^2}{\partial x_3^2}\Big[1-y_2\frac{\partial}{\partial x_2}\Big]B_1^{*(1)}(m_1,m_3=0)\Bigg\}$$

$$+\sum_{m_3=1}^{\infty}2i^{m_3+1}(-1)^{m_3}\Bigg\{\Big\|b_{21}^{*(1)}(n;m_1,m_3)\frac{\partial}{\partial x_3}\Big[1+y_2\frac{\partial}{\partial x_2}\Big]$$

$$+4\nu\kappa_n b_{31}^{*(1)}(n;m_1,m_3)\Big\|B^{*(2)}(m_1,m_3)+2\kappa_n b_{31}^{*(1)}(n;m_1,m_3)$$

$$\times\frac{\partial^2}{\partial x_3^2}\left[1-y_2\frac{\partial}{\partial x_2}\right]B_1^{*(1)}(m_1,m_3)\Big\}\Big),$$

$$\frac{u_2^{(3)A_n}(\vec{x})}{u_0(R)}=2\sum_{m_1=1}^{\infty}\Big((-1)^{m_1}-1\Big)\Bigg(\Big\|b_{21}^{*(1)}(n;m_1,m_3=0)\Big[(1+\nu)\frac{\partial}{\partial x_3}+y_2\frac{\partial^2}{\partial x_3\partial x_2}\Big]\frac{\partial}{\partial x_2}$$

$$+2\kappa_n b_{31}^{*(1)}(n;m_1,m_3=0)\Big[\nu\frac{\partial}{\partial x_2}-y_2\frac{\partial^2}{\partial x_3^2}\Big]\Big\|B_2^{*(1)}(m_1,m_3=0)$$

$$+\sum_{m_3=1}^{\infty}2i^{m_3}(-1)^{m_3}\Bigg\{\Big\|b_{21}^{*(1)}(n;m_1,m_3)\Big[(1+\nu)\frac{\partial}{\partial x_3}+y_2\frac{\partial^2}{\partial x_3\partial x_2}\Big]\frac{\partial}{\partial x_2}$$

$$+2\kappa_n b_{31}^{*(1)}(n;m_1,m_3)\Big[\nu\frac{\partial}{\partial x_2}-y_2\frac{\partial^2}{\partial x_3^2}\Big]\Big\|B_2^{*(1)}(m_1,m_3)\Bigg\}\Bigg),$$

$$\frac{u_3^{(3)A_n}(\vec{x})}{u_0(R)}=\sum_{m_1=1}^{\infty}\Big((-1)^{m_1}-1\Big)\Bigg(\Big\|b_{21}^{*(1)}(n;m_1,m_3=0)\Big[\frac{\partial^2}{\partial x_3^2}-2(1-\nu)\frac{\partial^2}{\partial x_2^2}$$

$$+y_2\frac{\partial^3}{\partial x_2\partial x_3^2}\Big]+4(2-\nu)\kappa_n b_{31}^{*(1)}(n;m_1,m_3=0)\frac{\partial}{\partial x_3}\Big\|B_2^{*(1)}(m_1,m_3=0)$$

$$+4(1-\nu)\kappa_n b_{31}^{*(1)}(n;m_1,m_3=0)\Big\|\frac{\partial^3}{\partial x_3^3}-y_2\frac{\partial^4}{\partial x_2\partial x_3^3}\Big\|B_3^{*(1)}(m_1,m_3=0)$$

$$+\sum_{m_3=1}^{\infty}2i^{m_3}(-1)^{m_3}\Bigg\{\Big\|b_{21}^{*(1)}(n;m_1,m_3)\Big[\frac{\partial^2}{\partial x_3^2}-2(1-\nu)\frac{\partial^2}{\partial x_2^2}+y_2\frac{\partial^3}{\partial x_2\partial x_3^2}\Big]$$

$$+4(2-\nu)\kappa_n b_{31}^{*(1)}(n;m_1,m_3)\frac{\partial}{\partial x_3}\Big\|B_2^{*(1)}(m_1,m_3)+4(1-\nu)\kappa_n b_{31}^{*(1)}(n;m_1,m_3)$$

$$\times\Big[\frac{\partial^3}{\partial x_3^3}-y_2\frac{\partial^4}{\partial x_2\partial x_3^3}\Big]B_3^{*(1)}(m_1,m_3)\Bigg\}\Bigg). \qquad (28)$$

$$u_1^{(2)A_n}(\vec{x})=u_0(R)\Bigg(\sum_{m_3=1}^{\infty}i^{m_3}\Big\{2b_{32}^{*(2)}(n;m_1=0,m_3)+\Delta b_{32}^{*(2)}(n;m_1=0,m_3)\Big\}$$

$$\times y_2\frac{\partial^2}{\partial x_1\partial x_3}B^{*(2)}(m_1=0,m_3)+\sum_{m_1=1}^{\infty}(-1)^{m_1+1}\Big[(-1)^{m_1}-1\Big]ib_{21}^{*(1)}(n;m_1,m_3=0)$$

$$\times\Big[-2(1-\nu)\frac{\partial}{\partial x_2}+y_2\frac{\partial^2}{\partial x_1^2}\Big]B^{*(2)}(m_1,m_3=0)+\sum_{m_3=1}^{\infty}i^{m_3}\Big\|\Big(1-(-1)^{m_1}\Big)(-1)^{m_3+1}$$

$$\times 2ib_{21}^{*(1)}(n;m_1,m_3)\left[-2(1-\nu)\frac{\partial}{\partial x_2}+y_2\frac{\partial^2}{\partial x_1^2}\right]-\left[\left((-1)^{m_1}+1\right)2b_{32}^{*(2)}(n;m_1,m_3)\right.$$

$$\left.+(-1)^{m_1}\Delta b_{32}^{*(2)}(n;-m_1,m_3)+\Delta b_{32}^{*(2)}(n;m_1,m_3)\right]y_2\frac{\partial^2}{\partial x_1\partial x_3}\left\|B^{*(2)}(m_1,m_3)\right\|\Bigg),$$

$$u_2^{(2)A_n}(\vec{x})=u_0(R)\Bigg(-\sum_{m_3=1}^{\infty}i^{m_3}\left\{2b_{32}^{*(2)}(n;m_1=0,m_3)+\Delta b_{32}^{*(2)}(n;m_1=0,m_3)\right\}$$

$$\times\left((1-2\nu-y_2\frac{\partial}{\partial x_2}\right)\frac{\partial}{\partial x_3}B^{*(2)}(m_1=0,m_3)+\sum_{m_1=1}^{\infty}(-1)^{m_1+1}\|i\left[1+(-1)^{m_1+1}\right]$$

$$\times b_{21}^{*(1)}(n;m_1,m_3=0)\left[1-2\nu-y_2\frac{\partial}{\partial x_2}\right]\frac{\partial}{\partial x_1}B^{*(2)}(m_1,m_3=0)$$

$$+\sum_{m_3=1}^{\infty}i^{m_3+1}\left\|\left[1-2\nu-y_2\frac{\partial}{\partial x_2}\right]\right\{2(-1)^{m_3}\left(1+(-1)^{m_1+1}\right)b_{21}^{*(1)}(n;m_1,m_3)\frac{\partial}{\partial x_1}$$

$$-i\left[2\left(1+(-1)^{m_1}\right)b_{32}^{*(2)}(n;m_1,m_3)+(-1)^{m_1}\Delta b_{32}^{*(2)}(n;-m_1,m_3)\right.$$

$$\left.+\Delta b_{32}^{*(2)}(n;m_1,m_3)\right]\frac{\partial}{\partial x_3}\Big\}\left\|B^{*(2)}(m_1,m_3)\right\|\Bigg),$$

$$\frac{u_3^{(2)A_n}(\vec{x})}{u_0(R)}=-\sum_{m_3=1}^{\infty}i^{m_3}\left\|2(1-\nu)\left\{2b_{32}^{*(2)}(n;m_1=0,m_3)+\Delta b_{32}^{*(2)}(n;m_1=0,m_3)\right\}\frac{\partial}{\partial x_2}\right.$$

$$\left.-y_2\left\{2b_{32}^{*(2)}(n;m_1=0,m_3)+\Delta b_{32}^{*(2)}(n;m_1=0,m_3)\right\}\frac{\partial^2}{\partial x_3^2}\right\|B^{*(2)}(m_1=0,m_3)$$

$$+\sum_{m_1=1}^{\infty}(-1)^{m_1+1}\|((-1)^{m_1}-1)ib_{21}^{*(1)}(n;m_1,m_3=0)y_2\frac{\partial^2}{\partial x_1\partial x_3}B^{*(2)}(m_1,m_3=0)$$

$$+\sum_{m_3=1}^{\infty}i^{m_3}\left\|2(1-\nu)\left\{2\left(1+(-1)^{m_1}\right)b_{32}^{*(2)}(n;m_1,m_3)+(-1)^{m_1}\Delta b_{32}^{*(2)}(n;-m_1,m_3)\right.\right.$$

$$\left.+\Delta b_{32}^{*(2)}(n;m_1,m_3)\right\}\frac{\partial}{\partial x_2}-y_2\left\{\left(1-(-1)^{m_1}\right)2i(-1)^{m_3}b_{21}^{*(1)}(n;m_1,m_3)\frac{\partial^2}{\partial x_1\partial x_3}\right.$$

$$+\left[\left(1+(-1)^{m_1}\right)2b_{32}^{*(2)}(n;m_1,m_3)+(-1)^{m_1}\Delta b_{32}^{*(2)}(n;-m_1,m_3)\right.$$

$$\left.\left.\left.+\Delta b_{32}^{*(2)}(n;m_1,m_3)\right]\frac{\partial^2}{\partial x_3^2}\right\}\right\|B^{*(2)}(m_1,m_3)\|; \qquad (29)$$

$$b_{32}^{*(2)}(n;m_1,m_3)-b_{32}^{*(2)}(n;m_1,-m_3)\equiv-\Delta b_{32}^{*(2)}(n;m_1,m_3)\,. \qquad (30)$$

$$\sigma_{ii}^{(m)A_n} = \frac{2\mu}{1-2\nu}\left(\left[\delta_{i1}(1-\nu)+\nu(\delta_{i2}+\delta_{i3})\right]\frac{\partial u_1^{(m)A_n}}{\partial x_1} \right.$$
$$\left. +\left[\delta_{i2}(1-\nu)+\nu(\delta_{i1}+\delta_{i3})\right]\frac{\partial u_2^{(m)A_n}}{\partial x_2}+\left[\delta_{i3}(1-\nu)+\nu(\delta_{i1}+\delta_{i2})\right]\frac{\partial u_3^{(m)A_n}}{\partial x_3}\right),$$
$$\sigma_{ij}^{(m)A_n} = \mu\left(\frac{\partial u_i^{(m)A_n}}{\partial x_j}+\frac{\partial u_j^{(m)A_n}}{\partial x_i}\right), \quad i \neq j; \tag{31}$$

III-2. Conoidal crack dislocation distributions

Assume first that the crack ***(Figure 1)*** is smooth ($\xi = 0$) and write the traction-free boundary condition (17) for positions P_C ($x_1 = R$, $x_2 = f = R\tan\theta$, $x_3 = 0$) with $x_3 = 0$. Hence in (17), $\partial f / \partial x_1 = \tan\theta$, $\partial f / \partial x_3 = x_3 \tan\theta / R = 0$ and $0 < R \leq a$. Denoting the associated dislocation distributions by $D_m^{(0)}$,

$$\sigma_{21}^a + \tan\theta\nu_A\sigma_{22}^a + \int_0^a \left(\sigma_{21}^{(1)(0)}(P_C;\overline{x}_1) - \tan\theta\sigma_{11}^{(1)(0)}(P_C;\overline{x}_1)\right)D_1^{(0)}(\overline{x}_1)d\overline{x}_1$$
$$+\int_0^a \left(\sigma_{21}^{(2)(0)}(P_C;\overline{x}_1) - \tan\theta\sigma_{11}^{(2)(0)}(P_C;\overline{x}_1)\right)D_2^{(0)}(\overline{x}_1)d\overline{x}_1 = 0,$$
$$\sigma_{22}^a + \tan\theta\sigma_{21}^a + \int_0^a \left(\sigma_{22}^{(1)(0)}(P_C;\overline{x}_1) - \tan\theta\sigma_{21}^{(1)(0)}(P_C;\overline{x}_1)\right)D_1^{(0)}(\overline{x}_1)d\overline{x}_1$$
$$+\int_0^a \left(\sigma_{22}^{(2)(0)}(P_C;\overline{x}_1) - \tan\theta\sigma_{21}^{(2)(0)}(P_C;\overline{x}_1)\right)D_2^{(0)}(\overline{x}_1)d\overline{x}_1 = 0,$$
$$\sigma_{23}^a + \int_0^a \left(\sigma_{32}^{(3)(0)}(P_C;\overline{x}_1) - \tan\theta\sigma_{31}^{(3)(0)}(P_C;\overline{x}_1)\right)D_3^{(0)}(\overline{x}_1)d\overline{x}_1 = 0. \tag{32}$$

Stress terms in (32) are given in *Appendix A*. Relations (32) consist of three singular integral equations the resolution of which provides the $D_m^{(0)}$ that depend on θ (see ***Figure 1*** for θ). $D_m^{(0)}$ may be used to approximate D_m as given by (17). Similar approximations have been used in previous works [5 – 9] to provide expressions for the crack extension force G when the crack fronts run indefinitely along the x_3- direction and spread in the plane perpendicular to the x_1 fracture propagation direction. For $\theta = 0$, $D_m^{(0)}$ ($\theta = 0$) correspond to the circular crack dislocation distributions that are available from [1] and will be used in the following.

III-3. Crack-tip stresses

The crack-tip stresses are required for the calculation of the crack extension force *G* (see *Section* 2). At an arbitrary position *P(R, ϕ)* (given by (1) with *R* between *R*= *a* (shorter crack) and *R*= *a* + δa (lengthened crack), $\delta a << a$) the crack-tip stresses separate into non-oscillatory and oscillatory terms as in (3). The formers are identified to the following formulae

$$\bar{\sigma}_{ij}^{(0)}(P) \equiv \sum_{m=1}^{3} \int_{a}^{a+\delta a} \sigma_{ij}^{(m)(0)}(P;\bar{x}_1) D_m(\bar{x}_1) d\bar{x}_1 \equiv \sum_{m=1}^{3} \bar{\sigma}_{ij}^{(m)(0)} \qquad (m = 1, 2 \text{ and } 3) \quad (33\,a)$$

in a similar way as in [1]; the oscillatory parts are given by

$$\bar{\sigma}_{ij}^{\xi}(P) \equiv \sum_{n} \sum_{m=1}^{3} \int_{a-\delta a}^{a} \sigma_{ij}^{(m)A_n}(P;\bar{x}_1) D_m(\bar{x}_1) d\bar{x}_1 \qquad (33\,b)$$

with following notations $\bar{\sigma}_{ij}^{\xi}(P) = \sum_{n} \sum_{m=1}^{3} \bar{\sigma}_{ij}^{(m)A_n} = \sum_{n} \bar{\sigma}_{ij}^{A_n} = \sum_{m=1}^{3} \bar{\sigma}_{ij}^{(m)\xi}$. These stress expressions mean that only those crack dislocations located about the crack front will contribute significantly to the stress at *P*; any other contribution becomes negligible for a sufficiently small value of δa. $\sigma_{ij}^{(m)(0)}(P;\bar{x}_1)$ is the non-oscillatory part of the stress at *P* due to a crack dislocation at an average elevation $\bar{h} = \bar{x}_1 \tan\theta$ (refer to ***Figure 1***); this corresponds to the stress of a circular dislocation. $\sigma_{ij}^{(m)A_n}(P;\bar{x}_1)$ is the oscillatory part of the stress at *P* due to a rough conoidal crack dislocation with form $A_n(\bar{x}_1, \phi)$ (refer to 1*a*) at an average elevation $\bar{h}$. D_m is obtained from (17); $D_m^{(0)}$ (32) may be used instead, writing

$$\bar{\sigma}_{ij}^{(m)(0)}(P) = \int_{a}^{a+\delta a} \sigma_{ij}^{(m)(0)}(P;\bar{x}_1) D_m^{(0)}(\bar{x}_1) d\bar{x}_1$$

$$\bar{\sigma}_{ij}^{(m)A_n}(P) = \int_{a-\delta a}^{a} \sigma_{ij}^{(m)A_n}(P;\bar{x}_1) D_m^{(0)}(\bar{x}_1) d\bar{x}_1 \cong \sigma_{ij}^{(m)A_n}(P;a) \int_{a-\delta a}^{a} D_m^{(0)}(\bar{x}_1) d\bar{x}_1 . \qquad (34)$$

δa *(<< a)* is small and will be made to go to zero in the calculation of the crack extension force. $\sigma_{ij}^{(m)(0)}(P;\bar{x}_1)$ and $\sigma_{ij}^{(m)A_n}(P;\bar{x}_1)$ are given in *Appendix B*.

III-4. Crack extension force for the rough circular crack ($\theta = 0$)

The crack extension force G (per unit length of the crack front) at an arbitrary position P_0 on the crack front is given by (25). For $\Delta u^{(i)}$ (24), we use (21) in which $D_m(\theta)$ is approximated by $D_m^{(0)}(\theta)$ solution of the singular integral equations (32). In the present work, G using $D_m^{(0)}(\theta = 0)$ is provided. Hence, this corresponds to a circular rough crack with average radius $R = a$ in the Ox_1x_3- plane. It is shown that only the non-oscillatory parts of the crack-tip stresses $\bar{\sigma}_{ij}^{(0)}$ (33*a*) contribute non-zero values to G. The oscillatory terms (33*b*) contribute nothing because they don't contain the appropriate singularity (of the Cauchy type in the crack dislocation stress fields) closer to the crack-tip. The rough circular crack extension force per unit length of the crack front shall be denoted $G_{RC}(P_0)$ at $P_0 \equiv P_D$ (1) with $h(a) = 0$ and $R = a$. We provide an associated normalized quantity $\tilde{G}_{RC}(P_0)$ defined as

$$\tilde{G}_{RC}(P_0) = G_{RC}(P_0) / G_C^{(I)},$$
$$G_C^{(I)} = \frac{8\alpha_0^2}{\pi^2} \ln\left(\frac{a}{\bar{a}}\right) G_0^I; \qquad (35)$$

$G_0^I = K_I^{0^2}(1-\nu^2)/E$, $K_I^0 = \sigma_{22}^a \sqrt{a\pi}$. The quantity in the logarithm is dimensionless, hence $\bar{a}$ is introduced with this respect; E is Young's modulus. $G_C^{(I)}$ is taken from [1] and represents a value of the crack extension force for the circular crack (centre O, radius a) in Ox_1x_3 under applied mode I loading. α_0 is a constant (see [1]). We write ($M_{12} = \sigma_{21}^a / \sigma_{22}^a$, $M_{13} = \sigma_{23}^a / \sigma_{22}^a$)

$$\tilde{G}_{RC}(P_0) = \sum_{j=1}^{3} \left(\tilde{G}_{1j}^{(1)(0)} + \tilde{G}_{2j}^{(2)(0)} + \tilde{G}_{3j}^{(3)(0)} \right); \qquad (36a)$$

$$\tilde{G}_{11}^{(1)(0)} = \frac{(2\ln 2 - 1)M_{12}}{8\ln(a/\bar{a})} \Bigg(2(1-2\nu)\sin^2\phi\, W_1^*(a,\phi) + \frac{\xi(a,\phi)}{a} \Big\{ 6W_1^*(a,\phi) \times \Big[-\sin\phi(1-4\cos^2\phi)M_{12} + \cos\phi(1-4\sin^2\phi)M_{13}/(1-\nu) \Big] - LN_1^*(a,\phi) \Big[\sin\phi(3-\cos^2\phi)M_{12} + \cos\phi(2\nu+\sin^2\phi)M_{13}/(1-\nu) \Big] \Big\} \Bigg),$$

$$\tilde{G}_{12}^{(1)(0)} = -\frac{(2\ln 2 - 1)M_{12}}{4\ln(a/\bar{a})} \Big(\overline{W}(a,\phi) \Big[(1-\nu\cos^2\phi)M_{12} + \nu \sin 2\phi M_{13}/\big(2(1-\nu)\big) \Big] + \big(\xi(a,\phi)/a\big)(1-\nu)\sin\phi\, \overline{LN}(a,\phi) \Big),$$

$$\tilde{G}_{13}^{(1)(0)} = -\frac{(2\ln 2-1)M_{12}}{8\ln(a/\bar{a})}\Bigg((1-2\nu)\sin 2\phi\, W_2^*(a,\phi) + \frac{\xi(a,\phi)}{a}\Big\{6W_2^*(a,\phi) \times\Big[\cos\phi(\cos^2\phi-3\sin^2\phi)M_{12}+\sin\phi(\sin^2\phi-3\cos^2\phi)M_{13}/(1-\nu)\Big] - LN_2^*(a,\phi)\Big[\cos\phi(1-\nu+\sin^2\phi)M_{12}+\sin\phi(1-\nu+\cos^2\phi)M_{13}/(1-\nu)\Big]\Big\}\Bigg),$$

$$\tilde{G}_{21}^{(2)(0)} = -\frac{(2\ln 2-1)}{4\ln(a/\bar{a})}\Big(W_1^*(a,\phi)\Big[(1-\nu\cos^2\phi)M_{12}+\nu\sin 2\phi M_{13}/\big(2(1-\nu)\big)\Big] + \big(\xi(a,\phi)/a\big)(1-\nu)\sin\phi LN_1^*(a,\phi)\Big),$$

$$\tilde{G}_{22}^{(2)(0)} = -\frac{2\ln 2-1}{8\ln(a/\bar{a})}\left(2(1-2\nu)\overline{W} - \frac{\xi(a,\phi)}{a}\overline{LN}\left[\sin\phi M_{12}+\frac{\cos\phi M_{13}}{1-\nu}\right]\right),$$

$$\tilde{G}_{23}^{(2)(0)} = \frac{(2\ln 2-1)}{4\ln(a/\bar{a})}\Big(W_2^*(a,\phi)\Big[\nu\sin 2\phi M_{12}/2+(1-\nu+\nu\cos^2\phi)M_{13}/(1-\nu)\Big] + \big(\xi(a,\phi)/a\big)(1-\nu)\cos\phi LN_2^*(a,\phi)\Big),$$

$$\tilde{G}_{31}^{(3)(0)} = \frac{(2\ln 2-1)M_{13}}{(1-\nu)8\ln(a/\bar{a})}\Bigg((1-2\nu)\sin 2\phi\, W_1^*(a,\phi) + \frac{\xi(a,\phi)}{a}\Big\{6W_1^*(a,\phi) \times\Big[\cos\phi(\cos^2\phi-3\sin^2\phi)M_{12}+\sin\phi(\sin^2\phi-3\cos^2\phi)M_{13}/(1-\nu)\Big] - LN_1^*(a,\phi)\Big[\cos\phi(1-\nu+\sin^2\phi)M_{12}+\sin\phi(1-\nu+\cos^2\phi)M_{13}/(1-\nu)\Big]\Big\}\Bigg),$$

$$\tilde{G}_{32}^{(3)(0)} = -\frac{(2\ln 2-1)M_{13}}{(1-\nu)4\ln(a/\bar{a})}\left(\overline{W}\left[\nu\sin 2\phi\frac{M_{12}}{2}+\left(1+\frac{\nu\cos^2\phi}{1-\nu}\right)M_{13}\right] + \frac{\xi(a,\phi)}{a}(1-\nu)\cos\phi\overline{LN}\right),$$

$$\tilde{G}_{33}^{(3)(0)} = -\frac{(2\ln 2-1)M_{13}}{(1-\nu)8\ln(a/\bar{a})}\Bigg(2(1-2\nu)\cos^2\phi\, W_2^*(a,\phi) + \frac{\xi(a,\phi)}{a}\Big\{6W_2^*(a,\phi) \times\Big[\sin\phi(\sin^2\phi-3\cos^2\phi)M_{12}+\cos\phi(3\sin^2\phi-\cos^2\phi)M_{13}/(1-\nu)\Big] - LN_2^*(a,\phi)\Big[\sin\phi(2\nu+\cos^2\phi)M_{12}+\cos\phi(3-\sin^2\phi)M_{13}/(1-\nu)\Big]\Big\}\Bigg); \quad (36b)$$

$$\overline{W}(a,\phi) = \frac{\cos\phi\big(1+\mathrm{sgn}(\sin\phi)\big)-\sin\phi\big(1-\mathrm{sgn}(\cos\phi)\big)}{\sqrt{1+\big(\partial\xi(a,\phi)/\partial R\big)^2+\big(\partial\xi(a,\phi)/\partial S\big)^2}},$$

$$\overline{LN}(a,\phi) = \frac{\ln\big\{(1+\cos\phi)(1-\sin\phi)\big\}/\big\{(1-\cos\phi)(1+\sin\phi)\big\}}{\sqrt{1+\big(\partial\xi(a,\phi)/\partial R\big)^2+\big(\partial\xi(a,\phi)/\partial S\big)^2}},$$

$$W_1^*(a,\phi)=\left(\sin\phi\frac{\partial\xi}{\partial R}(a,\phi)+\frac{\cos\phi}{a}\frac{\partial\xi}{\partial\phi}(a,\phi)\right)\overline{W}(a,\phi),$$

$$LN_1^*(a,\phi)=\left(\sin\phi\frac{\partial\xi}{\partial R}(a,\phi)+\frac{\cos\phi}{a}\frac{\partial\xi}{\partial\phi}(a,\phi)\right)\overline{LN}(a,\phi),$$

$$W_2^*(a,\phi)=\left(-\cos\phi\frac{\partial\xi}{\partial R}(a,\phi)+\frac{\sin\phi}{a}\frac{\partial\xi}{\partial\phi}(a,\phi)\right)\overline{W}(a,\phi),$$

$$LN_2^*(a,\phi)=\left(-\cos\phi\frac{\partial\xi}{\partial R}(a,\phi)+\frac{\sin\phi}{a}\frac{\partial\xi}{\partial\phi}(a,\phi)\right)\overline{LN}(a,\phi). \qquad (36c)$$

To graphical plots of $\tilde{G}_{RC}(P_0)$ (36), the special case of a sinusoidal crack front (use (1) for running point $P_0 \equiv P_D$ with $R = a$ and $h(a) = 0$) with

$$\xi(a,\phi)\equiv A_n(a,\phi)=\xi_n(a)\sin n|\phi|, \qquad |\phi|\le\pi, \qquad (37)$$

is analysed. ϕ_C, the crack-front inclination angle, is used with the following meaning: ϕ_C is the acute angle, at crack-front positions P_M located on the average crack plane, between the crack-front and the average fracture plane. Hence, for given R

$$\tan\phi_C=\frac{\partial A_n}{\partial S}(R,\phi)=\frac{1}{R}\frac{\partial A_n}{\partial\phi}=\frac{1}{R}\xi_n(R)n\,\mathrm{sgn}\,\phi\cos n\phi$$

Since $A_n(R, \phi) = 0$ at P_M and $\tan\phi_C$ positive, these lead to

$$\tan\phi_C=\frac{n}{R}\xi_n(R).$$

At any position with arbitrary R

$$A_n(R,\phi)=\frac{R}{n}\tan\phi_C\sin n|\phi|. \qquad (38)$$

We then write (37) as

$$\xi(a,\phi)=A_n(a,\phi)=\frac{a}{n}\tan\phi_C\sin n|\phi|. \qquad (39)$$

Under such conditions, the following average values for $\tilde{G}_{RC}$ (36) now denoted $<\tilde{G}_{RC}^{(S)}>$ for the sinusoidal crack-front are evaluated:

$$< \tilde{G}_{RC}^{(S)} >= \frac{1}{2\pi} \int_{-\pi}^{\pi} \tilde{G}_{RC}^{(S)}(P_0) d\phi = \frac{1}{\pi} \int_{-\pi/2}^{\pi/2} \tilde{G}_{RC}^{(S)}(P_0) d\phi \,. \quad (40)$$

$< \tilde{G}_{RC}^{(S)} >$ then depends on various parameters (ϕ_C; M_{12}, M_{13}; n, $a/\bar{a}$; ν). Extrema with respect to ϕ_C may also be measured using the relation

$$\frac{\partial}{\partial \phi_C} < \tilde{G}_{RC}^{(S)} >= 0 \,. \quad (41)$$

Figure 2 (*a*, *b* and ***c***) show plots of $< \tilde{G}_{RC}^{(S)} >$ (40) as a function of the couple (ϕ_C, M_{13}) for different values of the other parameters. No coloured regions of (ϕ_C, M_{13}) correspond to negative $< \tilde{G}_{RC}^{(S)} >$ (< 0); the associated crack configurations are not favoured. The coloured regions correspond to positive $< \tilde{G}_{RC}^{(S)} >$, indicating that the associated rough cracks can expand. (*b*) corresponds to (***a***) viewed in M_{13} magnitudes close to zero. Because M_{12} = 0.001 is small, it becomes apparent that rough sinusoidal circular cracks can expand under nearly pure applied tension for any ϕ_C. When M_{13} increases from zero, the non-planar crack motion becomes impossible except for large ϕ_C (say larger than 65°, approximately, in ***Figure* 2 *a and b***). Similar behaviours are present for larger n= 10 in ***Figure 2c***. Hence applied shearing stresses have the property of impeding the expansion of rough circular cracks. These latter cracks are mostly created under low shearing stresses.

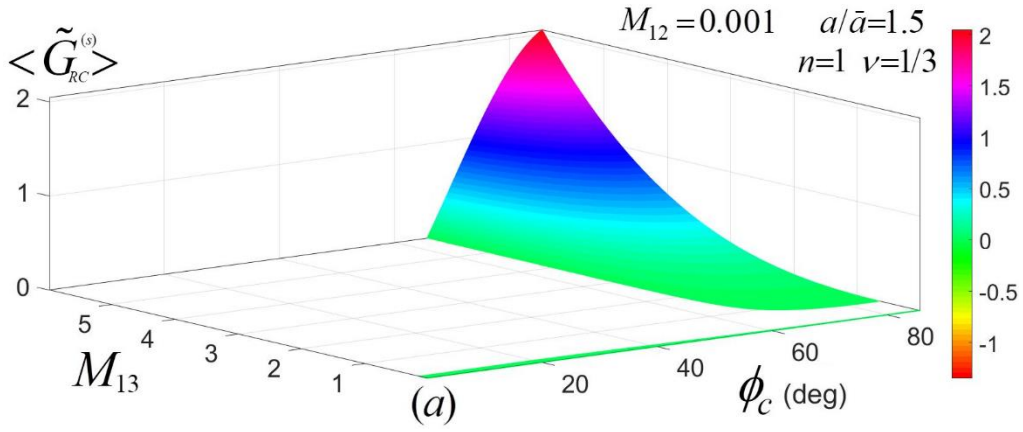

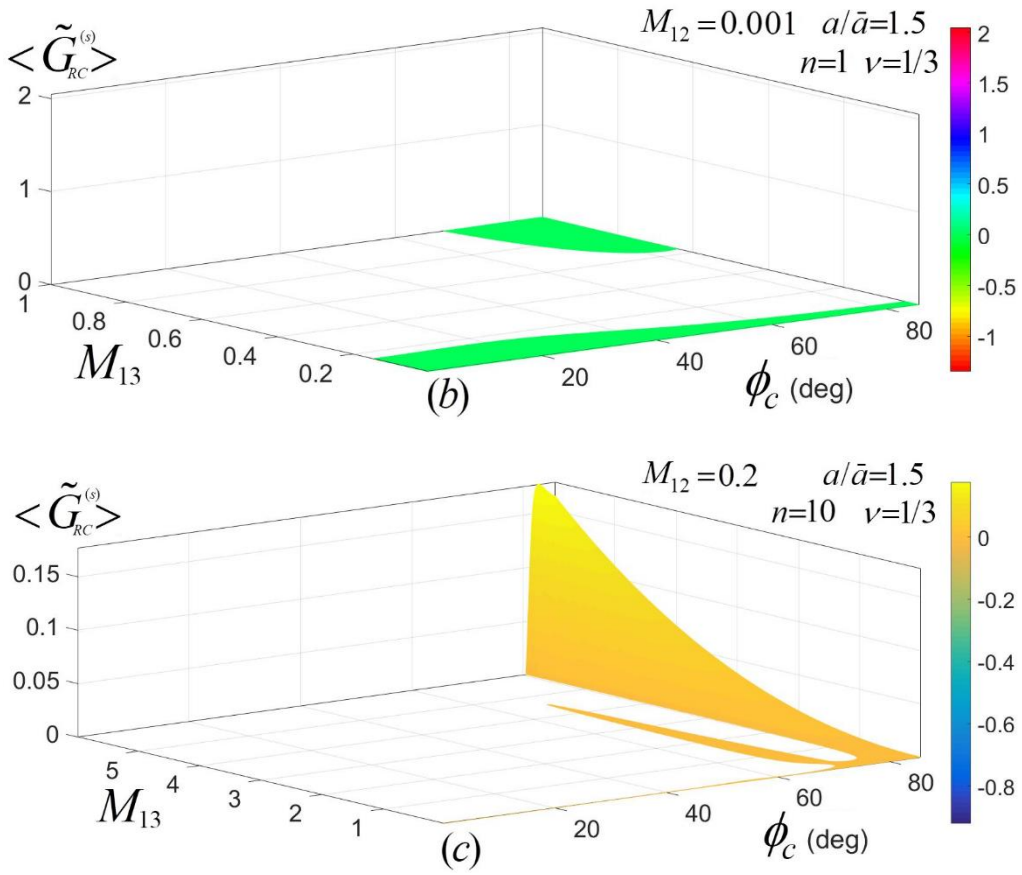

Figure 2 (*a*, *b* and *c*) : *Plots of the reduced crack extension force* $<\tilde{G}_{RC}^{(S)}>$ *(40) for the rough circular sinusoidal crack as a function of the pair of variables* (ϕ_C, M_{13}) *for different values of the other parameters* M_{12}, *n*, *v and* $a/\bar{a}$. *(b) corresponds to (a) viewed in magnitudes of* M_{13} *closer to zero. (c) corresponds to a larger n= 10 value.*

IV - DISCUSSION

A modelling of the rough conoidal crack ***(Figure 1)*** is presented that consists in representing the crack by a continuous distribution of dislocations with infinitesimal Burgers vectors *b*. The running position P_D along the dislocations is described by (1 *a* and *b*). Their elastic fields are given to linear terms with respect to the oscillations A_n or their spatial derivative $\partial A_n / \partial S$ along the crack front (*Section* 3.1). The crack dislocation distributions $D_m(\theta)$ provided by the traction-free crack face condition (17) are required to give explicit expressions of the crack-tip stresses and crack extension force. $D_m(\theta)$ is approximated by

$D_m^{(0)}(\theta)$ due to the smooth conoidal crack. The later are solutions of (32). The crack-tip stresses (34) are written as a function of $D_m^{(0)}(\theta)$ which remain to be determined at present. In the present work, to proceed further, we use $D_m^{(0)}(\theta = 0)$ [1] to calculate the crack extension force (36) for the rough circular cracks (*Section* 3.4). For plots, the special case of a sinusoidal crack front (37) is adopted involving the crack-front inclination angle ϕ_C (38, 39). Similar ϕ_C have been used in earlier works [5, 8] where the non-planar crack front is also sinusoidal; in these works, applied M_{13} have been found under which average crack extension force $< G >$ plotted as a function of ϕ_C exhibit positive maxima (see [5] and Figure 5 there, for example). The graphical representations of $\tilde{G}_{RC}^{(S)}$ (40) reveal that these types of non-planar closed crack loop can expand at small shearing stresses for all ϕ_C. With increasing M_{13} and M_{12}, their motions are unfavoured expect for large ϕ_C ($\geq 65°$, approximately). Characteristics that derive from ***Figure 2***, $D_m^{(0)}(\theta = 0)$, are expected to prevail for the general rough conoidal crack ($\theta \neq 0$), after inspection of the mathematics involved. On the experimental side, fracture surfaces of fatigued high strength steels in long-life regimes generally exhibit conoidal rough cracks, at the beginning of fracture initiation. These cracks have been named "fish-eyes" [10, 11].

The vertex of the conoidal rough crack is generally occupied by heterogeneities. An example of such fractured surface is displayed in ***Figure 3*** taken from [11]. ***Figure 3a*** shows a complete broken part of the cylindrical specimen in which the fish-eye is distinctly observed on the right of the micrograph and in ***Figure 3b***, its magnification. The vertex of the fish-eye is occupied by an AlN inclusion. Fracture develops first the rough conoidal crack over a diameter of 1*mm* approximately and further expands on a plane perpendicular to the loading axis. In the experiments by [11], no shearing stresses are applied. This agrees with the conclusion that the rough circular crack can be created under vanishing applied shearing stresses ***(Figure 2)***. Very similar fracture surface characteristics are present on SEM fractographic images of René 88DT specimens tested in fatigue at 650° C [12] : in their Figure 2(c) fracture produces, in order, a conoidal rough crack, a planar crack perpendicular to the tensile axis and lastly another planar surface that deviates notably from the preceding. We have shown [1] that, in addition to planar cracks perpendicular to the tensile axis, there exists planar fracture surfaces deviating from the formers by about 52°. From the experimental point of view, it is then possible to perform quantitative analyses of this mode of fatigue failure by linking the applied stresses to the number of cycles. This may be done empirically, first.

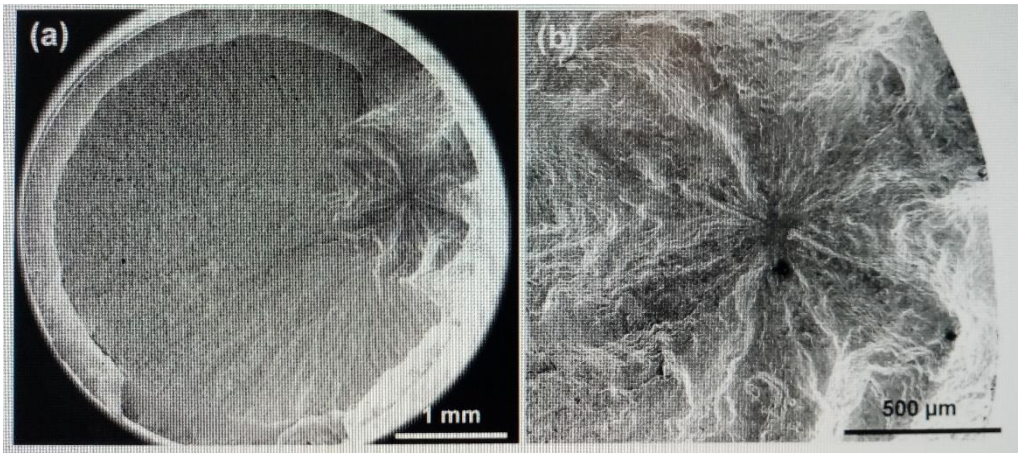

Figure 3 : (*a*) *Fracture surface of broken high strength steel specimen tested in fatigue at 20°C with the formation of a rough conoidal crack with an AlN inclusion located at its vertex. (b) Magnification of the conoidal crack (fish-eye). Micrographs are taken from* [11]

V - CONCLUSION

A way to analyse mathematically the rough conoidal crack under general loading is introduced. This consists in representing the complex crack by a continuous distribution of Volterra dislocations with infinitesimal Burgers vectors. This is a smooth cone on average, and for definiteness, with a vertex O at the origin, vertical symmetrical axis, horizontal circular basis at an elevation $x_2 = h(a)$ with radius $R = a$. Its surface consists of profound striations running radially to the vertex. The rough conoidal crack dislocation at the elevation $x_2 = h(R)$ ($R \leq a$) is obtained as the intersection of a vertical cylinder of radius R (axis x_2) and the rough crack. The dislocation distribution consists of three families (m) (distribution function D_m; $m = 1$, 2 and 3) with burgers vectors $\boldsymbol{b}_m$ directed along the positive x_m- directions. The stresses are applied uniformly at infinity with tension σ_{22}^a along x_2 and shears σ_{21}^a and σ_{23}^a along x_1 and x_3. Poisson's normal stresses $-\nu\sigma_{22}^a$ (ν is Poisson's ratio) acting in the x_1 and x_3 directions are incorporated into the analysis. Plastic distortions associated with these dislocations are first given and corresponding expressions of the associated elastic fields (displacement and stress) are also provided (*Section* 3.1). Then distribution function $D_m^{(0)}$ of circular horizontal dislocations (with the identical Burgers vectors b_m) covering the smooth conoidal crack are considered and three singular integral equations that

determine $D_m^{(0)}$ are written down (*Section* 3.2). $D_m^{(0)} = D_m^{(0)}(\theta)$ depends on angle θ, complementary to the half angle at the vertex of the cone. $D_m^{(0)}$ may be used to approximate D_m. The crack-tip stresses have been given as functions of $D_m^{(0)}$. Explicit expressions of the rough circular crack extension force G_{RC} per unit length of the crack front are given that are associated with $D_m^{(0)}$ (θ=0). Expressions $< \tilde{G}_{RC}^{(S)} >$ of $G_{RC}^{(S)}$ (crack extension force) averaged over the length of the oscillatory crack-front are plotted for the special case of sinusoidal fronts. These plots reveal that the rough circular cracks can expand under small shearing stresses. Agreements are found with long-life fatigue experiments in high strength materials.

REFERENCES

[1] - P. N. B. ANONGBA, Elliptical crack under arbitrarily applied loadings : dislocation, crack-tip stress and crack extension force, *Rev. Ivoir. Sci. Technol.*, 38 (2021) 388 - 409

[2] - T. MURA, The continuum theory of dislocations, In : "Advances in Materials Research" (Edited by H. Herman), *Interscience Publications*, Vol. 3, (1968) 1 - 108

[3] - T. MURA, "Micromechanics of defects in Solids", Martinus Nijhoff Publishers, Dordrecht, (1987)

[4] - B. A. BILBY and J. D. ESHELBY, Dislocations and the theory of fracture, In : "Fracture", Ed. Academic Press (H. Liebowitz), New York, Vol. 1, (1968) 99 - 182

[5] - P. N. B. ANONGBA, An analysis of a non-planar crack under mixed mode I + III loading using infinitesimal dislocations with edge and screw average characters, *ResearchGate*, DOI : 10.13140/RG.2.2.14308.60806

[6] - P. N. B. ANONGBA, A study of the mixed mode I+III loading of a non-planar crack using infinitesimal dislocations, *Rev. Ivoir. Sci. Technol.*, 14 (2009) 55 - 86

[7] - P. N. B. ANONGBA, Non-planar crack under general loading : dislocation, crack-tip stress and crack extension force, *Rev. Ivoir. Sci. Technol.*, 16 (2010) 11 - 50

[8] - P. N. B. ANONGBA, Non-planar interface crack under general loading : III. Dislocation, crack-tip stress and crack extension force, *Rev. Ivoir. Sci. Technol.*, 32 (2018) 10 - 47

[9] - P. N. B. ANONGBA, Non-planar cracks in uniform motion under general loading, *Rev. Ivoir. Sci. Technol.*, 36 (2020) 119 - 149

[10] - T. SAKAI, N. OGUMA and A. MORIKAWA, Characteristic S-N properties of high-carbon-chromium-bearing steel under axial loading in long-life fatigue, *Fatigue Fract Engng Mater Struct*, 25 (2002) 765 - 773

[11] - H. ABDESSELAM et al., On the crystallographic, stage I like, character of fine granular area formation internal fish-eye fatigue cracks, *Int J Fatigue*, 106 (2018) 132 - 142

[12] - J. C. STINVILLE et al., Fatigue deformation in a polycrystalline nickel base superalloy at intermediate and high temperature: competing failure modes, *Acta Materialia*, 152 (2018) 16 - 33

APPENDIX A : STRESS TERMS IN (32) (*SECTION* 3.2)

Under $x_1 \neq \overline{x}_1$, we have

$$\sigma_{21}^{(1)(0)}(P_C;\overline{x}_1)-\tan\theta\sigma_{11}^{(1)(0)}(P_C;\overline{x}_1)=C_1\frac{\overline{x}_1}{2}\int_{-\infty}^{\infty}\int_{-\infty}^{\infty}e^{-\tan\theta|x_1-\overline{x}_1|\eta_1}J_1[\overline{x}_1\eta_1]e^{ik_1x_1}dk_1dk_3$$
$$\times\left(\nu-1+\frac{1}{\eta_1}\left\{\tan\theta|x_1-\overline{x}_1|k_1^2-i2\tan\theta\,\mathrm{sgn}(x_1-\overline{x}_1)k_1\right.\right.$$
$$\left.\left.+\frac{1}{\eta_1}\left[i\tan^2\theta(x_1-\overline{x}_1)k_1^3-\nu k_1^2\right]\right\}\right),$$

$$\sigma_{21}^{(2)(0)}(P_C;\overline{x}_1)-\tan\theta\sigma_{11}^{(2)(0)}(P_C;\overline{x}_1)=C_1\overline{x}_1\int_{-\infty}^{\infty}\int_{-\infty}^{\infty}\frac{J_1[\overline{x}_1\eta_1]}{\eta_1}e^{ik_1x_1}dk_1dk_3$$
$$\times\left((1-\nu)H\left[x_1-\overline{x}_1\right]ik_1+e^{-\tan\theta|x_1-\overline{x}_1|\eta_1}\left\{(1-\nu)\mathrm{sgn}(x_1-\overline{x}_1)ik_1\right.\right.$$
$$\left.\left.+\tan^2\theta|x_1-\overline{x}_1|(k_1^2+2\nu k_3^2)/\left[2(1-2\nu)\right]-(1-2\nu)\tan\theta k_1^2/(2\eta_1)\right\}\right);$$

$$\sigma_{22}^{(1)(0)}(P_C;\overline{x}_1)-\tan\theta\sigma_{21}^{(1)(0)}(P_C;\overline{x}_1)=C_1\frac{\overline{x}_1}{2}\int_{-\infty}^{\infty}\int_{-\infty}^{\infty}e^{-\tan\theta|x_1-\overline{x}_1|\eta_1}J_1[\overline{x}_1\eta_1]e^{ik_1x_1}dk_1dk_3$$
$$\times\tan\theta\left(1-\nu+(x_1-\overline{x}_1)ik_1+\frac{k_1^2}{\eta_1}\left\{\frac{\nu}{\eta_1}-\tan\theta|x_1-\overline{x}_1|\right\}\right),$$

$$\sigma_{22}^{(2)(0)}(P_C;\overline{x}_1)-\tan\theta\sigma_{21}^{(2)(0)}(P_C;\overline{x}_1)=C_1\overline{x}_1\int_{-\infty}^{\infty}\int_{-\infty}^{\infty}\frac{J_1[\overline{x}_1\eta_1]}{\eta_1}e^{ik_1x_1}dk_1dk_3$$
$$\times\left((\nu-1)\tan\theta H\left[x_1-\overline{x}_1\right]ik_1-e^{-\tan\theta|x_1-\overline{x}_1|\eta_1}\left\{(1-\nu)\tan\theta\,\mathrm{sgn}(x_1-\overline{x}_1)ik_1\right.\right.$$
$$\left.\left.+\eta_1\left[(1-2\nu)^2+\tan\theta|x_1-\overline{x}_1|\eta_1\right]/\left[2(1-2\nu)\right]\right\}\right);$$

$$\sigma_{32}^{(3)(0)}(P_C;\bar{x}_1)-\tan\theta\sigma_{31}^{(3)(0)}(P_C;\bar{x}_1)=C_1\frac{\bar{x}_1}{2}\int_{-\infty}^{\infty}\int_{-\infty}^{\infty}e^{-\tan\theta|x_1-\bar{x}_1|\eta_1}\frac{J_1[\bar{x}_1\eta_1]}{\eta_1}e^{ik_1x_1}dk_1dk_3$$
$$\times\Bigg((\nu-1)\tan\theta\,\mathrm{sgn}(x_1-\bar{x}_1)ik_1+\tan\theta|x_1-\bar{x}_1|k_3^2-\eta_1$$
$$+\frac{k_1}{\eta_1}\left[\nu k_1+\tan^2\theta(x_1-\bar{x}_1)ik_3^2\right]\Bigg);$$

$C_1=\mu b/2\pi(1-\nu)$, μ is the shear modulus and H the Heaviside step function.

APPENDIX B : STRESSES FOR THE CRACK-TIP

$\sigma_{ij}^{(m)(0)}(P;\bar{x}_1)$ (34) are listed below; these are written to linear terms with respect to $(x_2-\bar{h})$, small quantity different from zero $(x_2-\bar{h}\neq 0)$

$$\sigma_{11}^{(1)(0)}(P;\bar{x}_1)=C_1\bar{x}_1 2\Bigg(-\mathrm{sgn}(x_2-\bar{h})2\int_0^{\pi/2}\sin\psi L_1^*d\psi$$
$$+(x_2-\bar{h})\int_0^{\pi/2}\sin\psi(2+\sin^2\psi)M_2^*d\psi\Bigg),$$
$$\sigma_{22}^{(1)(0)}(P;\bar{x}_1)=-C_1\bar{x}_1(x_2-\bar{h})2\int_0^{\pi/2}\sin\psi M_2^*d\psi,$$
$$\sigma_{33}^{(1)(0)}(P;\bar{x}_1)=C_1\bar{x}_1 2\Bigg(-2\nu\,\mathrm{sgn}(x_2-\bar{h})\int_0^{\pi/2}\sin\psi L_1^*d\psi$$
$$+(x_2-\bar{h})\int_0^{\pi/2}\sin\psi\left[1+2\nu-\sin^2\psi\right]M_2^*d\psi\Bigg),$$
$$\sigma_{21}^{(1)(0)}(P;\bar{x}_1)=C_1\bar{x}_1 2\Bigg(-\int_0^{\pi/2}\left(1-\nu+\nu\sin^2\psi\right)M_1^*d\psi$$
$$+|x_2-\bar{h}|\int_0^{\pi/2}\left[1-\nu+(1+\nu)\sin^2\psi\right]L_2^*d\psi\Bigg),$$

$$\sigma_{13}^{(1)(0)}(P;\bar{x}_1)=C_1\bar{x}_1 2\left(-(1-\nu)\operatorname{sgn}(x_2-\bar{h})\int_0^{\pi/2}\cos\psi L_1^* d\psi\right.$$
$$\left.+(x_2-\bar{h})\int_0^{\pi/2}\cos\psi\left[1-\nu+\sin^2\psi\right]M_2^* d\psi\right),$$

$$\sigma_{23}^{(1)(0)}(P;\bar{x}_1)=-C_1\bar{x}_1\left(\nu\int_0^{\pi/2}\sin 2\psi M_1^* d\psi+(1-\nu)\left|x_2-\bar{h}\right|\int_0^{\pi/2}\sin 2\psi L_2^* d\psi\right);$$

$$\sigma_{11}^{(2)(0)}(P;\bar{x}_1)=-\frac{2C_1\bar{x}_1}{1-2\nu}\left(-(1-2\nu)^2\int_0^{\pi/2}\sin^2\psi M_1^* d\psi\right.$$
$$\left.+2\left|x_2-\bar{h}\right|\int_0^{\pi/2}\left[\nu+(1-\nu)(1-2\nu)\sin^2\psi\right]L_2^* d\psi\right),$$

$$\sigma_{22}^{(2)(0)}(P;\bar{x}_1)=-\frac{2C_1\bar{x}_1}{1-2\nu}\left((1-2\nu)^2\int_0^{\pi/2}M_1^* d\psi+4\nu(1-\nu)\left|x_2-\bar{h}\right|\int_0^{\pi/2}L_2^* d\psi\right),$$

$$\sigma_{33}^{(2)(0)}(P;\bar{x}_1)=-\frac{2C_1\bar{x}_1}{1-2\nu}\left(-(1-2\nu)^2\int_0^{\pi/2}\cos^2\psi M_1^* d\psi\right.$$
$$\left.+2\left|x_2-\bar{h}\right|\int_0^{\pi/2}\left[\nu^2+(1-\nu)\left\{\nu+(1-2\nu)\cos^2\psi\right\}\right]L_2^* d\psi\right),$$

$$\sigma_{12}^{(2)(0)}(P;\bar{x}_1)=C_1 4(1-\nu)\bar{x}_1\left(-\left\{H(x_2-\bar{h})+\operatorname{sgn}(x_2-\bar{h})\right\}\int_0^{\pi/2}\sin\psi L_1^* d\psi\right.$$
$$\left.+(x_2-\bar{h})\int_0^{\pi/2}\sin\psi M_2^* d\psi\right),$$

$$\sigma_{13}^{(2)(0)}(P;\bar{x}_1)=C_1\bar{x}_1\left((1-2\nu)\int_0^{\pi/2}\sin 2\psi M_1^* d\psi-2(1-\nu)\left|x_2-\bar{h}\right|\int_0^{\pi/2}\sin 2\psi L_2^* d\psi\right),$$

$$\sigma_{23}^{(2)(0)}(P;\bar{x}_1)=C_1 4(1-\nu)\bar{x}_1\left(-\left\{H(x_2-\bar{h})+\operatorname{sgn}(x_2-\bar{h})\right\}\int_0^{\pi/2}\cos\psi L_1^* d\psi\right.$$

$$+(x_2-\bar{h})\int_0^{\pi/2}\cos\psi M_2^* d\psi\Bigg);$$

$$\sigma_{11}^{(3)(0)}(P;\bar{x}_1)=C_1 2\bar{x}_1\Bigg(-2\nu\,\mathrm{sgn}(x_2-\bar{h})\int_0^{\pi/2}\cos\psi L_1^* d\psi$$

$$+(x_2-\bar{h})\int_0^{\pi/2}\cos\psi\left[2\nu+\sin^2\psi\right]M_2^* d\psi\Bigg),$$

$$\sigma_{22}^{(3)(0)}(P;\bar{x}_1)=-C_1 2\bar{x}_1(x_2-\bar{h})\int_0^{\pi/2}\cos\psi M_2^* d\psi,$$

$$\sigma_{33}^{(3)(0)}(P;\bar{x}_1)=C_1 2\bar{x}_1\Bigg(-2\,\mathrm{sgn}(x_2-\bar{h})\int_0^{\pi/2}\cos\psi L_1^* d\psi$$

$$+(x_2-\bar{h})\int_0^{\pi/2}\cos\psi(2+\cos^2\psi)M_2^* d\psi\Bigg),$$

$$\sigma_{12}^{(3)(0)}(P;\bar{x}_1)=\sigma_{23}^{(1)(0)},$$

$$\sigma_{13}^{(3)(0)}(P;\bar{x}_1)=C_1 2\bar{x}_1\Bigg(-(1-\nu)\,\mathrm{sgn}(x_2-\bar{h})\int_0^{\pi/2}\sin\psi L_1^* d\psi$$

$$+(x_2-\bar{h})\int_0^{\pi/2}\sin\psi\left[1-\nu+\cos^2\psi\right]M_2^* d\psi\Bigg),$$

$$\sigma_{23}^{(3)(0)}(P;\bar{x}_1)=C_1 2\bar{x}_1\Bigg(-\int_0^{\pi/2}\left(1-\nu+\nu\cos^2\psi\right)M_1^* d\psi$$

$$+\left|x_2-\bar{h}\right|\int_0^{\pi/2}\left[1-\nu+(1+\nu)\cos^2\psi\right]L_2^* d\psi\Bigg); \qquad \text{(B1)}$$

$$M_1^*=\begin{cases}\bar{x}_1/\left(\bar{x}_1^2-\Omega^2\right)^{3/2} & for\ \Omega^2/\bar{x}_1^2<1\\ 0 & \Omega^2/\bar{x}_1^2\geq 1\end{cases},$$

$$M_2^*=\begin{cases}-3\bar{x}_1\Omega/\left(\bar{x}_1^2-\Omega^2\right)^{5/2} & for\ \Omega^2/\bar{x}_1^2<1\\ 0 & \Omega^2/\bar{x}_1^2\geq 1\end{cases},$$

$$L_1^* = \begin{cases} 0 & \Omega^2/\bar{x}_1^2 \le 1 \\ -\bar{x}_1/\left(\Omega^2-\bar{x}_1^2\right)^{3/2} & for\ \Omega^2/\bar{x}_1^2 > 1 \end{cases},$$

$$L_2^* = \begin{cases} 0 & \Omega^2/\bar{x}_1^2 \le 1 \\ 3\bar{x}_1\Omega/\left(\Omega^2-\bar{x}_1^2\right)^{5/2} & for\ \Omega^2/\bar{x}_1^2 > 1 \end{cases},$$

$$\Omega = R\cos(\phi-\psi). \qquad \text{(B2)}$$

For $x_2-\bar{h}=0$ corresponding to positions $P\equiv P_M$ (x_1= R sinϕ, $x_2=\bar{h}=\bar{x}_1\tan\theta$, x_3= R cosϕ) (see (34)), the stresses $\sigma_{ij}^{(m)(0)}(P_M,\bar{x}_1)$ are due to a circular smooth dislocation parallel to x_1x_3 with radius $\bar{x}_1$, displaced vertically by $x_2=\bar{h}(\bar{x}_1)$ from the initial centre O. They may be calculated from [1]. The oscillatory parts of the crack-tip stress fields $\bar{\sigma}_{ij}^{(m)An}(P)$ (34) (m= 1, 2 and 3) contribute zero to the crack extension force. This is because the stresses $\sigma_{ij}^{(m)An}(P;a)$ do not contain a singularity of the Cauchy-type; these are bounded. Below are displayed results for crack dislocation family m= 3 only. Expressions for the others are similar. To the linear order with respect to ξ_n,

$$\sigma_{ii}^{(3)An}(P;\bar{x}_1)=0 \quad (i=1,\ 2\ \text{and}\ 3), \qquad \sigma_{13}^{(3)An}(P;\bar{x}_1)=0,$$

$$\bar{\sigma}_{23}^{(3)\xi}(P)=\frac{C_1}{\pi}\sum_{s,s_1,s_3=0}^{\infty}(-1)^{s_3}\Big\|a2(2s+1)\xi_{n=2s+1}(a)\,\mathrm{sgn}\,A_{2s+1}(R,\phi)$$
$$\times\left(2-\delta_{0(2s_3)}\right)\bar{b}_{21}^{*(1)}(n=2s+1;m_1,m_3=2s_3)I_{23}^{(3)}(1)-2\left\{2s\xi_{2s}(a)\,\mathrm{sgn}\,A_{2s}(R,\phi)\right.$$
$$\times\left(2-\delta_{0(2s_3)}\right)\bar{b}_{31}^{*(1)}(n=2s;m_1,m_3=2s_3)I_{23}^{(3)}(3)+2(2s+1)\xi_{2s+1}(a)\,\mathrm{sgn}\,A_{2s+1}(R,\phi)$$
$$\left.\times\bar{b}_{31}^{*(1)}(n=2s+1;m_1,m_3=2s_3+1)I_{23}^{(3)}(4)\right\}\Big\|\int_{a-\delta a}^{a}D_3^{(0)}(\bar{x}_1)d\bar{x}_1,$$

$$\bar{\sigma}_{21}^{(3)\xi}(P)=\frac{C_1}{\pi}\sum_{s,s_1,s_3=0}^{\infty}(-1)^{s_3}\Big\|a(2+\nu)2(2s+1)\xi_{n=2s+1}(a)\,\mathrm{sgn}\,A_{2s+1}(R,\phi)$$
$$\times\left(2-\delta_{0(2s_3)}\right)\bar{b}_{21}^{*(1)}(n=2s+1;m_1,m_3=2s_3)I_{21}^{(3)}(1)+2\nu\left\{2s\xi_{2s}(a)\,\mathrm{sgn}\,A_{2s}(R,\phi)\right.$$
$$\times\left(2-\delta_{0(2s_3)}\right)\bar{b}_{31}^{*(1)}(n=2s;m_1,m_3=2s_3)I_{21}^{(3)}(3)+2(2s+1)\xi_{2s+1}(a)\,\mathrm{sgn}\,A_{2s+1}(R,\phi)$$
$$\left.\times\bar{b}_{31}^{*(1)}(n=2s+1;m_1,m_3=2s_3+1)I_{21}^{(3)}(4)\right\}\Big\|\int_{a-\delta a}^{a}D_3^{(0)}(\bar{x}_1)d\bar{x}_1; \qquad \text{(B3)}$$

$$m_1=2s_1+1\ , \quad \delta_{0(2s_3)}=\begin{cases}1 & for\ s_3=0\\ 0 & s_3\neq 0\end{cases},$$

$$I_{23}^{(3)}(1)=4\int_0^{\pi/2}\frac{(2+\nu)\cos^2\psi+1-\nu}{\sin\psi}I_1^*(m_1=2s_1+1,m_3=2s_3)d\psi\,,$$

$$I_{23}^{(3)}(3)=4\int_0^{\pi/2}\frac{\cos\psi}{\sin\psi}I_2^*(m_1=2s_1+1,m_3=2s_3)d\psi\,,$$

$$I_{23}^{(3)}(4)=4\int_0^{\pi/2}\frac{\cos\psi}{\sin\psi}I_2^*(m_1=2s_1+1,m_3=2s_3+1)d\psi\,,$$

$$I_{21}^{(3)}(1)=4\int_0^{\pi/2}\cos\psi I_1^*(m_1=2s_1+1,m_3=2s_3)d\psi\,,$$

$$I_{21}^{(3)}(3)=4\int_0^{\pi/2}I_2^*(m_1=2s_1+1,m_3=2s_3)d\psi\,,$$

$$I_{21}^{(3)}(4)=4\int_0^{\pi/2}I_2^*(m_1=2s_1+1,m_3=2s_3+1)d\psi\,,$$

$$I_1^*(P;a;m_1,m_3)=\frac{(-1)^{s_1+s_3}a^{m_1+m_3}}{2^{m_1+m_3}m_3!}\frac{1}{(x_1+(\tan\psi)^{-1}x_3)^{m_1}(\tan\psi x_1+x_3)^{m_3}\Omega^3}$$

$$\times\sum_{k=0}^{\infty}(m_1+m_3+2k+2)!\frac{a^{2k}}{2^{2k}(x_1+(\tan\psi)^{-1}x_3)^{2k}}\frac{F\left(-k,-m_1-k;m_3+1;(\tan\psi)^{-2}\right)}{k!(m_1+k)!}$$

,

$$I_2^*(P;a;m_1,m_3)=\frac{(-1)^{s_1+s_3+1}a^{m_1+m_3}}{2^{m_1+m_3}m_3!}\frac{1}{(x_1+(\tan\psi)^{-1}x_3)^{m_1}(\tan\psi x_1+x_3)^{m_3}\Omega^2}$$

$$\times\sum_{k=0}^{\infty}(m_1+m_3+2k+1)!\frac{a^{2k}}{2^{2k}(x_1+(\tan\psi)^{-1}x_3)^{2k}}\frac{F\left(-k,-m_1-k;m_3+1;(\tan\psi)^{-2}\right)}{k!(m_1+k)!}$$

;

F is Gauss's hypergeometric function.